Ocean Science Journal, Vol. 41 No. 1, 1-10(2006)

Article

Ocean Science Journal

http://osj.kordi.re.kr

The Characteristics of Signal versus Noise SST Variability in the North Pacific and the Tropical Pacific Ocean

Sang-Wook Yeh[1]* and Ben P. Kirtman[2]

[1]*Ocean Circulation and Climate Research Division, KORDI, Ansan P.O. Box 29, Seoul 425-600, Korea*

[2]*Center for Ocean-Land-Atmosphere Studies, Institute of Global Environment and Society, George Mason University, 4041 Powder Mill Rd., Suite 302 Calverton, MD 20705, U.S.A.*

Received 28 December 2005; Revised 8 February 2006; Accepted 23 March 2006

Abstract – Total sea surface temperature (SST) in a coupled GCM is diagnosed by separating the variability into signal variance and noise variance. The signal and the noise is calculated from multi-decadal simulations from the COLA anomaly coupled GCM and the interactive ensemble model by assuming both simulations have a similar signal variance. The interactive ensemble model is a new coupling strategy that is designed to increase signal to noise ratio by using an ensemble of atmospheric realizations coupled to a single ocean model. The procedure for separating the signal and the noise variability presented here does not rely on any ad hoc temporal or spatial filter. Based on these simulations, we find that the signal versus the noise of SST variability in the North Pacific is significantly different from that in the equatorial Pacific. The noise SST variability explains the majority of the total variability in the North Pacific, whereas the signal dominates in the deep tropics. It is also found that the spatial characteristics of the signal and the noise are also distinct in the North Pacific and equatorial Pacific.

Key words – North Pacific, Equatorial Pacific, signal and noise, interactive ensemble model, SST variability

1. Introduction

Atmospheric variability in seasonal-to-interannual time scales is often analyzed by separating it into an internal component based on atmospheric dynamics only and an external (or forced) component based on the variability of sea surface temperature (SST) forcing. Traditionally, these two modes of atmospheric variability have been identified by performing an ensemble of independent long-term simulations of the atmospheric response to be observed or prescribed SST (Hannachi 2001; Shukla *et al.* 2000; Straus and Shukla 2000; Hoerling *et al.* 1997; Zwiers 1996; Harzallah and Sadourny 1995 among many others). An ensemble of atmospheric simulations is performed in which each integration, begun from different initial conditions, experiences the same evolution of the prescribed SST boundary condition. The forced variability is defined from the analysis of the ensemble mean and the internal variability is estimated by subtracting the ensemble mean from each ensemble member.

However, this method is limited to the analysis of atmospheric variables and can only be applied to separate an SST-forced signal and climate noise. Our goal here is to separate the SST variability into signal and noise components without any ad hoc temporal or spatial filter. This separation relies on a new strategy for coupling state-of-the-art oceanic general circulation models (OGCMs) and atmospheric general circulation models (AGCMs; Kirtman and Shukla 2002). The interactive ensemble strategy is to couple multiple realizations of a particular AGCM to a single OGCM. Ensemble averaging is applied to the air-sea fluxes of heat, momentum, and freshwater thereby significantly reducing the 'noise' in the fluxes applied to the ocean component without affecting the atmospheric internal dynamics fluctuations that are unrelated to the SST anomalies (SSTAs). The approach is to extend this notion of ensemble averaging to a coupled model with the expressed purpose of reducing the variability that is

*Corresponding author. E-mail: swyeh@kordi.re.kr

forced by the internal atmospheric dynamics. This extension of ensemble averaging is distinct from the traditional approach in that ensemble averaged atmospheric states are coupled to a single ocean model realization (Kirtman and Shukla 2002) as opposed to ensemble multiple coupled model realizations.

The standard coupled model has one AGCM coupled to one OGCM; however, this new interactive ensemble strategy has six realizations of the AGCM coupled to a single realization of the OGCM. As the interactive ensemble evolves, each AGCM realization experiences the same SST predicted by the OGCM. The OGCM, on the other hand, experiences surface fluxes that are the ensemble average of the six AGCM realizations. By comparing the variability of the interactive ensemble model with the standard coupled model, it is possible to separate the signal and noise in the total SST variability.

In constructing this separation it is assumed that the interactive ensemble technique reduces the noise, but has no impact on the signal. In this paper, we show the characteristics of the signal versus the noise SST variability in the North Pacific and the tropical Pacific Ocean. Our results show that the signal and the noise components of SST variability are markedly different in these two regions.

2. Model and Methodology

Both the standard coupled model and the interactive ensemble model combined the Center for Ocean-Land-Atmosphere Studies (COLA) GCM and the Geophysical Fluid Dynamics Laboratory (GFDL) Modular Ocean Model (MOM), version 3.0, ocean GCM. Brief descriptions of these models are given below.

Atmosphere model

A number of changes to the atmospheric model have been made since the original coupled models were developed. The dynamic core used in the National Center for Atmospheric Research (NCAR) Community Climate Model (CCM) version 3.0 has been adopted (Schneider 2001). The dynamic core is spectral (truncated at total triangular wavenumber 42) with semi-Lagrangian transport. There are 18 unevenly spaced sigma-coordinate vertical levels. The parameterization of the solar radiation is after Breigleb (1992) and terrestrial radiation follows Harshvardhan *et al.* (1987). The deep convection is an implementation of the Relaxed Arakawa-Schubert scheme of Moorthi and Suarez (1992) described by Dewitt (1996). The convective cloud fraction follows the scheme used by the NCAR CCM (Kiehl *et al.* 1994; see DeWitt and Schneider 1996 for additional details). There is a turbulent closure scheme for the subgrid scale exchange of heat, momentum, and moisture as in Miyakoda and Sirutis (1977) and Mellor and Yamada (1982). Additional details regarding the AGCM physics can be found in Kinter *et al.* (1988) and Dewitt (1996).

Ocean model

The ocean model is version 3 of the GFDL MOM (Pacanowski and Griffies 1998), a finite difference treatment of the primitive equations of motion using the Boussinesq and hydrostatic approximations in spherical coordinates. The domain is that of the World Ocean between 74°S and 65°N. The coastline and bottom topography are realistic except that ocean depths less than 100 m are set to 100 m and the maximum depth is set to 6000 m. The artificial high-latitude meridional boundaries are impermeable and insulating. The zonal resolution is 1.5. The meridional grid spacing is 0.5 between 10°S and 10°N, gradually increasing to 1.5 at 30°N and 30°S and fixed at 1.5 in the extratropics. There are 25 levels in the vertical mixing scheme is the non-local K-profile parameterization of Large *et al.* (1994). The horizontal mixing of tracers and momentum is Laplacian. The momentum mixing uses the space-time dependent scheme of Smagorinky (1963) and the tracer mixing used Redi (1982) diffusion along with Gent and McWilliams (1990) quasi-adiabatic stirring. The vertical mixing used Pacanowski and Philander (1981) in a Pacific basin only domain.

Coupling strategies

The anomaly coupling strategy is described in detail in Kirtman *et al.* (1997). Kirtman *et al.* (2002) showed that the anomaly coupling strategy guarantees that the climatology of the coupled model is close to the observed climatology. The main idea is that the ocean and atmosphere exchanged predicted anomalies, which are computed relative to their own model climatologies, while the climatology upon which the anomalies are superimposed is specified from observations. The anomaly coupling strategy requires atmospheric model climatologies of momentum, heat and fresh water flux, and an ocean model SST climatology.

Similarly, observed climatologies of momentum, heat and fresh water flux and SST are also required. The model climatologies are defined by separate uncoupled extended simulations of the ocean and atmospheric models. In the case of the atmosphere, the model climatology is computed from a 30-year (1961-1990) integration with observed specified SST. This SST is also used to define the observed SST climatology. In the case of the ocean model SST climatology, an extended uncoupled ocean model simulation is made using 30 years of 1000 mb National Center for Environmental Prediction (NCEP) reanalysis winds. The NCEP winds are converted to a wind stress following Trenberth *et al.* (1990). As with the SST, this observed wind stress product is used to define the observed momentum flux climatology. The heat flux and the fresh water flux in this ocean only simulation is parameterized using damping of SST and sea surface salinity to observed conditions with a 100 day time scale. The heat and fresh water flux "observed" climatologies are then calculated from the results of the extended-only simulation. The ocean and atmosphere model exchange daily mean flux and SST once a day.

In order to separate the signal versus noise SST variability, the simulated SST from both the standard coupled model (hereafter, SC) and interactive ensemble model (hereafter, IE) are used. Both simulations have been run for more than 200 years and all of the analysis shown here is based on the SST data for the last 200 years.

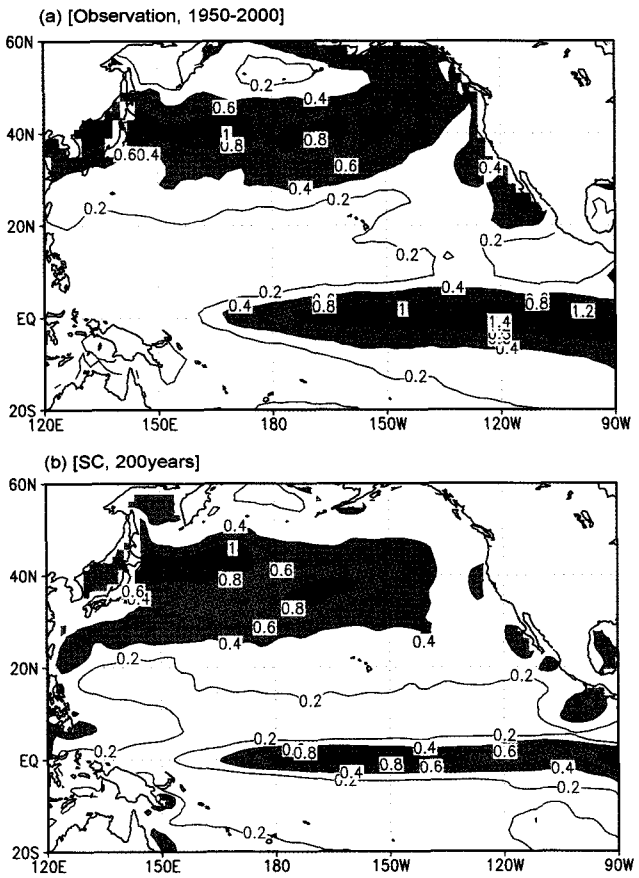

Fig. 1. The total SSTA variability for the observations for the period of 1950-2000 (a) and (b) as in (a) except for the standard coupled model for the period of 200 yrs. Contour interval is 0.2[°C]^2. Shading is for above 0.4[°C]^2.

3. Total SSTA Variability in the Pacific

Figure 1 shows the total SSTA variability for the observations and the SC model. The observed SST data are from January 1950 to December 2000 (Reynolds and Smith 1994). The anomaly is defined as the deviation from the mean annual cycle calculated over the entire record for each field. The total SSTA variability both for the observations and SC model has two regions of prominent variability: a band of SSTA variability centered near 40°N and a narrow band of high variability in the equatorial region from 5°S-5°N.

The band of strong SSTA variability centered near 40°N stretches from the coast of Asia into the central North Pacific for both the observations and SC model although the center of maximum SSTA variability is slightly shifted to the north in the SC model. This variability is closely connected to the dominant decadal SSTA variability in the North Pacific although it has also significant variability on interannual time scales. Based on filtered (Period > 7 yr) SST data taken from the COADS (Comprehensive Ocean-Atmosphere Data Set), Nakamura *et al.* (1997) found that there is strong decadal variability which was concentrated around the two major oceanic fronts within the North Pacific basin. The strongest variability is found around the subarctic front extending zonally at 42°N. This region of variability is associated with the subpolar gyre including the Kuroshio-Oyashio extension (KOE). The second maximum of the variability nearly coincides with the subtropical front which is oriented from the northeast to the southwest. It is also known that the spatial pattern of the SSTA variability associated with the Pacific decadal oscillation is more zonally elongated and extends

all the way across the North Pacific basin (Seager *et al.* 2001, Zhang *et al.* 1997; Tanimoto *et al.* 1997). Power spectra (not shown) from the SC model data yields significant decadal variability in the North Pacific region (140°E-210°E, 35°N-45°N) which is in good agreement with the observations.

The SSTA variability in the equatorial Pacific is strongest between 5°S-5°N in both the SC model and the observations, although the model variability is weak and is too narrowly confined to the equator. This meridional scale problem in coupled GCMs has been noted in many other coupled simulations (*e.g.* Kirtman and Zebiak 1997). Within the tropical Pacific basin, the variability is dominated by the El Nino-Southern Oscillation (ENSO) on the interannual time scales. The standard coupled model produces irregular ENSO events that are qualitatively similar to the observed events in terms of their period and amplitude (Kirtman *et al.* 2002). Overall, the SC model has reasonably realistic simulation of the dominant decadal SST variability in the North Pacific and interannual variability in the equatorial Pacific.

4. SST Signal versus Noise in the Pacific

In separating the SST signal and the SST noise we make two assumptions. First, the signal is independent from the noise; therefore, the total SSTA variability can be represented as the sum of the signal and the noise. This approach is similar to the statistical tool which is employed to separate the total atmospheric variability of SST-forced signal and random internal variability in long-term ensemble simulations (Rowell 1998 and many others). Second, we assume that the signal in the SC and the IE models is the same, and that the noise in the IE simulation is one sixth of the SC. This is because the IE simulation experiences surface fluxes that are the ensemble average of six atmospheric realizations. In essence, we assume that all the SST noise variability changes in proportion to the amplitude of the atmospheric noise variability. These assumptions lead us to the following decomposition of the total SSTA variability in the SC and the IE model.

Total SST variability: SC = S + N (S: *Signal*, N: *Noise*)
Total SST variability: IE = S + N/6

Because we know the total SST variability in each case, the SST signal and the noise variability can be calculated from the above relationships. Despite the simplicity of this formulation, it is found that this decomposition is reasonable when applied to the wind stress, and is conservative when compared with the traditional approach for determining the signal and the noise (see the Appendix). As mentioned in the introduction, the traditional approach is from a posteriori ensemble averaging of multiple coupled model realizations; however, the decomposition used in this study is based on the ensemble averaging applied to the wind stress as the coupled system evolves.

Based on the above formulation, Fig. 2 shows the spatial pattern of the signal and the noise SSTA variability in the North Pacific. The total SSTA variability in the North Pacific is almost entirely due to the noise except in regions of higher latitude than 50°N. Nevertheless, there is some detectable signal in the North Pacific. The spatial structure of the signal and the noise have some interesting similarities. The SST signal variability has two regions showing prominent variance: (i) a band that extends from the east of Japan to the central North Pacific near the date line and (ii) a weaker signal that is orientated to the northeast-southwest in the region of 180°E-150°W, 30°N-40°N. Similar to the signal variability, the noise SST variability has also its local maxima in the above two regions. As mentioned above, these two regions in the

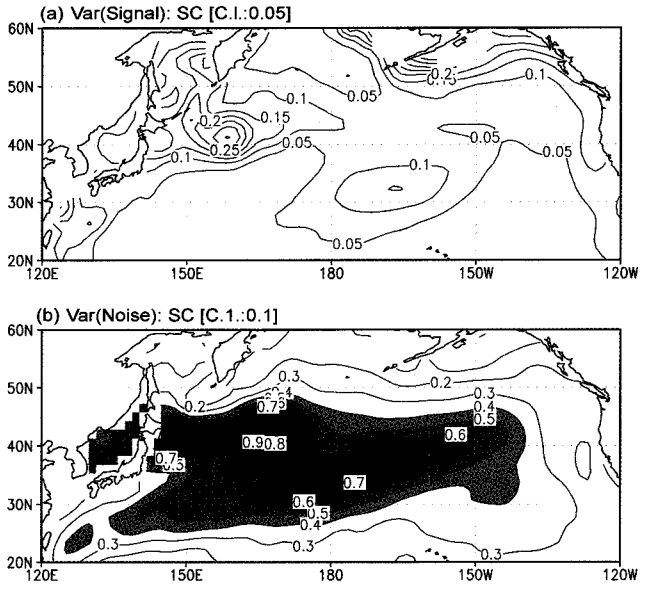

Fig. 2. The spatial pattern of signal (a) and noise (b) SSTA variability for the North Pacific in the standard coupled model. Unit is $[°C]^2$. Shading is for above $0.4[°C]^2$. Note the different contour intervals on the two panels.

North Pacific are also the regions with strong decadal SST variability, which regions are connected to major oceanic frontal zones with the subpolar and subtropical gyre, respectively.

Barnett *et al.* (1999) argued that the Kuroshio current, its extension, and the entire subtropical gyre are deeply involved in the Pacific decadal oscillation. Based on examining an ocean model forced by observed wind stress, Miller *et al.* (1998) showed that the North Pacific subpolar gyre, which is related to the KOE, and the subtropical gyre strengthened from the 1970s to the 1980s. Our result suggests that both oceanic gyres, which are closely connected to the North Pacific decadal variability are mostly associated with SSTA noise variability.

Figure 3 shows the ratio of the signal versus the noise SSTA variability in the North Pacific. The ratio between the signal and the noise SSTA variance is on the order of 0.1~0.3 except in the high latitude region around 50°N. This result suggests that stochastic midlatitude atmospheric forcing determines 70-90% of the SSTA variability in the North Pacific. Early studies of local ocean-atmosphere interaction by Davis (1976) and Frankignoul and Hasselmann (1977) suggested a red-noise type of correlation between atmospheric forcing and SST patterns, with the ocean passively responding to atmospheric forcing. Hasselmann (1976) also argued that an important feature of the climate system is the red noise oceanic response to white noise atmospheric forcing. Recent studies by many other investigators reached a similar conclusion, that atmospheric forcing on the ocean played the dominant role (Battisti *et al.* 1995; Delworth 1996; Saravanan and McWilliams 1995; Saravanan 1998). Our result indicates that this concept is valid for atmosphere-ocean interactions in the North Pacific. However, we cannot make any conclusions for the origin of SSTA variability in the high latitude region. The stochastic forcing, the ocean noise or unstable coupled feedback may play a significant role over there.

We found similar results when these analyses were applied to the results in the interactive ensemble model (not shown) in which the OGCM experiences surface fluxes that are the ensemble average of the twelve AGCM realizations (Yeh and Kirtman 2004). Yeh and Kirtman (2004) argued that the amplitude of internal atmospheric variability at air-sea interfaces decreases proportionally to the increasing of number of AGCM realizations, indicating that the SSTA variability in the North Pacific is much forced by the internal atmospheric dynamics.

Not surprisingly, the relative contribution of the signal versus the noise in the equatorial region is completely different compared to that of the North Pacific. Figure 4 is the same as in Fig. 2 except for the equatorial Pacific. In the deep Tropics, the signal dominates the noise; however, the signal to noise ratio falls rapidly poleward. In contrast to the North Pacific, the tropical atmosphere either has relatively less noise or the noise is relatively ineffective in forcing SSTA variability suggesting that tropical atmosphere-ocean system is more highly coupled.

In contrast to the signal and noise characteristics in the North Pacific, that of signal and the noise are different each other in the equatorial Pacific. The signal is narrowly confined to the equator, whereas the noise is relatively less equatorially trapped in the eastern Pacific. Figures

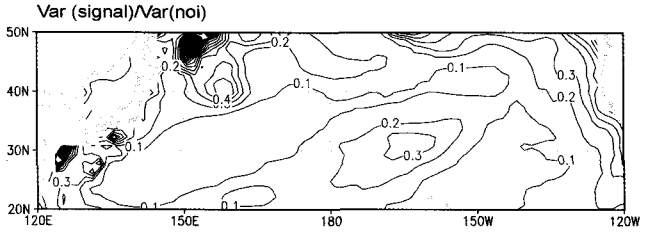

Fig. 3. The ratio of the signal versus the noise SSTA variance in the North Pacific in the standard coupled model. Unit is nondimensional.

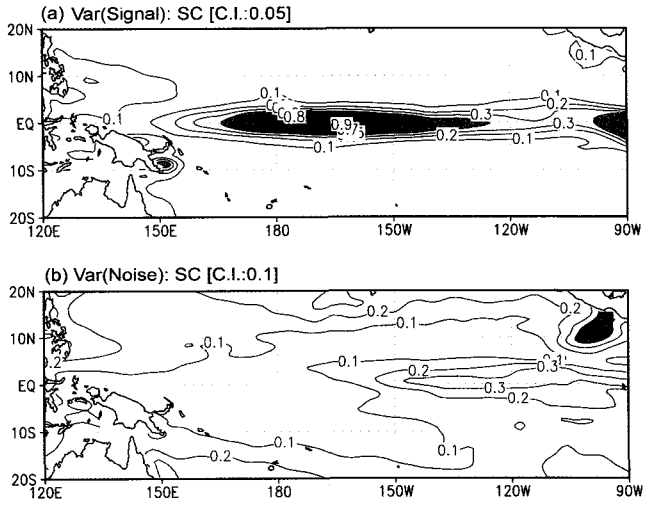

Fig. 4. The spatial pattern of signal (a) and noise (b) SSTA variability for the equatorial Pacific in the standard coupled model. Contour interval is 0.1[°C]^2. Shading is for above 0.4[°C]^2.

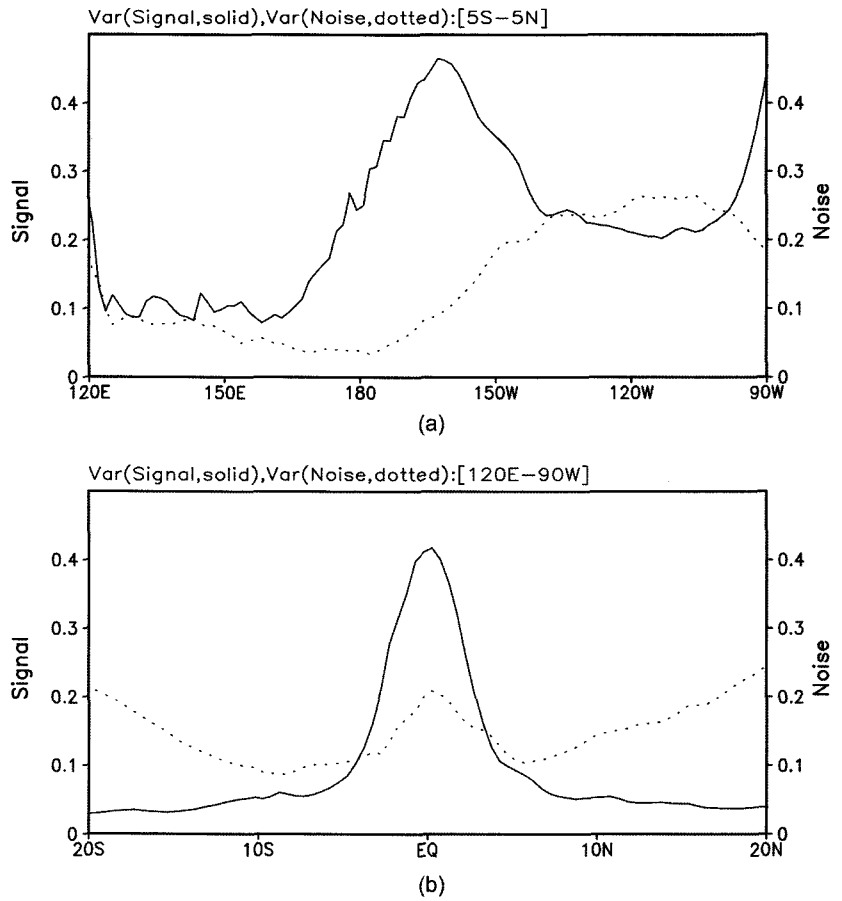

Fig. 5. The signal (solid) and the noise (dotted) averaged in the zonal band (5°N-5°S) in the equatorial Pacific (a) and (b) as in (a) except for the meridional band (120°E-90°W). Unit is $[°C]^2$. Note that the amplitude of the signal (noise) is indicated on the left (right) of each panel.

5a,b shows the zonal (a) and meridional structure (b) of the signal and the noise variance averaged in 5°N-5°S, 120°E-90°W, respectively. Note that the amplitude of the noise is indicated on the right of each panel. The signal variance is narrowly confined an equatorial band (Fig. 5b) and it is dominant in two regions: one is the central Pacific around 180°E-150°W and the other is trapped in the far eastern coast of South America (Fig. 5a). On the other hand, the noise variability is less equatorially confined (Fig. 5b) and is almost equal to the signal variance in the eastern Pacific between 150°W and 100°W (Fig. 5a). These characteristics of the signal and the noise patterns are distinct from those of North Pacific where the signal and noise variance were collocated. It is also interesting to note that in the eastern Pacific, where the model variability is weak compared to observations, the noise variability is comparable to the signal.

5. Concluding Remarks

By using a new coupling strategy, we have devised a simple formulation for isolating SST signal and noise variance. This is a new approach for determining how much SST variability is signal and how much is noise and does not rely on ad hoc temporal or spatial filter. We briefly compared characteristics of the signal and the noise variability in the North Pacific and equatorial Pacific. The relative contribution of the signal versus the noise in the both Pacific regions is different. The noise (signal) SSTA variability dominates in the North (equatorial) Pacific.

Although there is a large difference in magnitude, both the signal and the noise in the North Pacific are concentrated to the two regions that are related to the major oceanic fronts. The signal variance and the noise

variance are collocated. There is no consensus as to whether decadal variability in the midlatitudes involves a coupled ocean-atmosphere mode rather than merely reflecting forcing of the ocean by stochastic variability (Alexander 1992; Miller *et al.* 1998; Latif and Barnett 1994, 1996; Robertson 1996; Barnett *et al.* 1999). The result of the ratio of the signal and the noise versus the total SSTA variability suggests that the midlatitude ocean system is primarily responding to atmospheric noise and that the signal is quite small. This means that coupled ocean-atmosphere processes are difficult to detect in the North Pacific, and even if detected, their contribution is on the order of 10-20% of the total variability. On the other hand, this result also suggests that there is coupled ocean-atmosphere variability in the North Pacific on the order of 10-20% of the total variance that may be predictable.

In contrast to the North Pacific, the tropical ocean-atmosphere system is highly coupled. Analysis of the spatial pattern of the variance indicates that the signal and the noise in the equatorial Pacific are out of phase. The region showing minimum signal variability is coincident to that of maximum noise variability in the equatorial band. The coupled model variability in the eastern Pacific is particularly weak compared to the observations. It is interesting to note that this is a region where the signal and noise variability are comparable. It is our speculation that since the thermocline simulation is particularly poor in this region, i.e., too close to the surface, the ocean is very sensitive to atmospheric noise. Another possible interpretation is that the SST is less predictable in the far eastern Pacific, which is becoming part of the conventional wisdom based on coupled model prediction. In other words, the NINO3.4 (5°N-5°S, 170°E-120°W) index is more predictable than the NINO3 (5°N-5°S, 150°W-90°W) index.

Acknowledgments

S.-W. Yeh is grateful to Dr. I.-U. Chung and Dr. C.-J. Jang who provided many suggestions that have improved this manuscript. This research was supported by grants from the National Science Foundation ATM-9814295 and ATM-0122859, the National Oceanic and Atmospheric Administration NA16-GP2248 and National Aeronautics and Space Administration NAG5-11656. S.-W. Yeh is supported by KORDI (PE96200, PE97005 and PP06401).

References

Alexander, M.A. 1992. Midlatitude atmosphere-ocean interaction during El Nino, I. The North Pacific Ocean. *J. Climate*, **5**, 944-958.

Barnett, T.P., D.W. Pierce, R. Saravanan, N. Schneider, D. Dommenget, and M. Latif. 1999. Origins of the midlatitude Pacific decadal variability. *Geophys. Res. Lett.*, **26**, 1454-1456.

Battisti, D.S., U.S. Bhatt, and M.A. Alexander. 1995. A modeling study of interannual variability in the wintertime North Atlantic Ocean. *J. Climate*, **8**, 3067-3083.

Briegleb, B.P. 1992. Delta-Eddington approximation for solar radiation in the NCAR community climate model. *J. Geopys. Res.*, **97**, 7603-7612.

Davis, R.E. 1976. Predictability of sea surface temperature anomalies and sea level pressure anomalies over the North Pacific ocean. *J. Phys. Oceanogr.*, **6**, 249-266.

Delworth, T. 1996. North Atlantic interannual variability in a coupled ocean-atmosphere model. *J. Climate*, **9**, 2356-2375.

DeWitt, D.G. 1996. The effect of the cumulus convection on the climate of the COLA general circulation model. COLA Tech. Rep. 27. 69 p.

DeWitt, D.G. and E.K. Schneider. 1996. The Earth radiation budget as simulated by the COLA GCM. COLA Tech. Rep. 35. 39 p.

Frankignoul, C. and K. Hasselmann. 1977. Stochastic climate models: Part I. Application to sea surface temperature anomalies and thermocline variability. *Tellus*, **29**, 289-305.

Gent, P.R. and J.C. McWilliams. 1990. Isopycnal mixing in ocean circulation models. *J. Phys. Oceanogr.*, **20**, 150-155.

Hannachi, A. 2001. Toward a nonlinear identification of the atmospheric response to ENSO. *J. Climate*, **14**, 2138-2149.

Hasselmann, K. 1976. Stochastic climate models: Part I. Theory. *Tellus*, **28**, 473-485.

Harshvardhan, R.R. Davis, D.A. Randall, and T.G. Corsetti. 1987. A fast radiation parameterization for general circulation models. *J. Geophys. Res.*, **92**, 1009-1016.

Harzallah, A. and R. Sadourny. 1995. Internal versus SST-forced atmospheric variability as simulated by an atmospheric general circulation model. *J. Climate*, **8**, 474-495.

Hoerling, M.P., A. Kumar, and M. Zhong. 1977. El Nino, La Nina, and the nonlinearity of their teleconnections. *J. Climate*, **10**, 1769-1786.

Kiehl, J.T., J.J. Hack, and B.P. Briegleb. 1994. The simulated earth radiation budget of the National Center for Atmospheric Research community climate model CCM2 and comparisons with the Earth Radiation Budget Experiment (ERBE). *J. Geophy. Res.*, **99**, 20815-20827.

Kinter, J.L. III, J. Shukla, L. Marx, and E.K. Schneider. 1988. A simulation of winter and summer circulations with the NMC global spectral model. *J. Atmos. Sci.*, **45**, 2468-2522.

Kirtman, B.P. and J. Shukla. 2002. Interactive coupled ensemble: A new coupling strategy for CGCMs. *Geophys. Res. Lett.*, **29**, 1029-1032.

Kirtman, B.P., Y. Fan, and E.K. Schneider. 2002. The COLA global coupled and anomaly coupled ocean-atmosphere GCM. *J. Climate*, **15**, 2301-2320.

Kirtman, B.P. and S. Zebiak. 1997. ENSO simulation and prediction with a hybrid coupled model. *Mon. Wea. Rev.*, **125**, 2620-2641.

Large, W.G., J.C. McWilliams, and S.C. Doney. 1994. Oceanic vertical mixing: A review and a model with a nonlocal boundary layer parameterization. *Rev. Geophys.*, **32**, 363-403.

Latif, M. and T.P. Barnett. 1994. Causes of decadal climate variability over the North Pacific and North America. *Science*, **266**, 634-637.

Miller, A.J., D.R. Cayan, and W.B. White. 1998. A westward-intensified decadal change in the North Pacific thermocline and gyre-scale circulation. *J. Climate*, **11**, 3112-3127.

Miyakoda, K. and J. Sirutis. 1977. Comparative integrations of global spectral models with various parameterized processes of sub-grid scale vertical transport. *Beitr. Phys. Atmos.*, **50**, 445-480.

Moorthi, S. and M.J. Suarez. 1992. Relaxed Arakawa-Schubert: A parameterization of moist convection for general circulation models. *Mon. Wea. Rev.*, **120**, 978-1002.

Nakamura, H., G. Lin, and T. Yamagata. 1997. Decadal climate variability in the North Pacific during the recent decades. *Bull. Amer. Meteor. Soc.*, **78**, 2215-2225.

Pacanowski, R.C., K. Dixon, and A. Rosati. 1993. The GFDL modular ocean model users guide, version 1.0. GFDL Ocean Group Tech Rep. No. 2. 77 p.

Pacanowski, R.C. and S.M. Griffies. 1998. MOM 3.0 manual. NOAA/Geophysical Fluid Dynamics Laboratory. 638 p.

Redi, M.H. 1982. Oceanic isopycnal mixing by coordinate rotation. *J. Phys. Oceanogr.*, **12**, 1155-1158.

Reynolds, R. and T. M. Smith. 1994. Improved global sea surface temperature analysis using optimum interpolation. *J. Climate*, **7**, 929-948.

Robertson, A.W. 1996. Interdecadal variability over the North Pacific in a multi-century climate simulation. *Climate Dyn.*, **12**, 227-241.

Rosati, A. and K. Miyakoda. 1988. A general circulation model for upper ocean circulation. *J. Phys. Oceanogr.*, **18**, 1601-1626.

Rowell, D.P. 1998. Assessing potential seasonal predictability with an ensemble of multidecadal GCM simulations. *J. Climate*, **11**, 109-120.

Saravanan, R. 1998. Atmospheric low-frequency variability and its relationship to midlatitude SST variability: Studies and the NCAR Climate System Model. *J. Climate*, **11**, 1386-1404.

Saravanan, R. and J.C. McWilliams. 1995. Multiple equilibria, natural variability, and climate transitions in an idealized ocean-atmosphere model. *J. Climate*, **8**, 2296-2323.

Schneider, E.K. 2002. Causes of differences between the equatorial Pacific as simulated by two coupled GCMs. *J. Climate*, **15**, 2301-2320.

Seager, R., Y. Kushnir, N.H. Naik, M.A. Cane, and J. Miller. 2001. Wind-driven shifts in the latitude of the Kuroshio-Oyashio extension and generation of SST anomalies on decadal timescales. *J. Climate*, **15**, 4249-4265.

Shukla, J. and co-authors. 2000. Dynamical seasonal prediction. *Bull. Amer. Meteor. Soc.*, **81**, 2593-2606.

Smagorinsky, J. 1963. General circulation experiments with the primitive equations. I. The basic experiment. *Mon. Wea. Rev.*, **91**, 99-164.

Straus D.M. and J. Shukla. 2000. Distinguishing between the SST-forced variability and internal variability in mid-latitudes: Analysis of observation and GCM simulations. *Quart. J. Roy. Meteorol. Soc.*, **126**, 2323-2350.

Tanimoto, Y., N. Iwasaka, and K. Hanawa. 1997. Relationships between sea surface temperature, the atmospheric circulation and air-sea fluxes on multiple timescales. *J. Meteor. Soc. Jpn.*, **75**, 831-849.

Yeh, S.-W. and Ben P. Kirtman. 2004. The impact of internal atmospheric variability on the North Pacific SST variability. *Climate Dyn.*, **22**, 721-732.

Zhang, Y., J.M. Wallace, and D.S. Battisti. 1997. ENSO-like interdecadal variability: 1900-93. *J. Climate*, **10**, 1004-1020.

Zwiers, F.W. 1996. Interannual variability and predictability in an ensemble of AMIP climate simulations conducted with the CCC GCM2. *Climate Dyn.*, **12**, 825-847.

Appendix

This appendix presents the signal and noise calculation applied to the zonal wind stress. Since this is atmospheric-variable, it is available for each of the six ensemble members in the IE. The intent is to check the methodology introduced in section 4 against a more traditional approach. The traditional method for separating the signal and noise from the wind stress based on the six AGCM realizations in the IE model simulation. By total variation, we mean the total sum of squares, $TSS = \sum_{N=1}^{6} \sum_{T}^{200yr} (WS_{NT} - \overline{WS_{OO}})^2$ of the monthly mean wind stress computed across all realizations and years. Here, WS_{NT} indicates the monthly mean wind stress in each month (T) of simulation N, and $\overline{WS_{OO}}$ is the ensemble climatology computed by averaging across all years and simulations. We used the two-way analysis of variance technique to calculate the noise variability (Zwiers 1996). The noise variability measures the internal or natural variation of the variable and the signal is taken by subtracting the noise from the total variation (TSS).

$$Noise = \sum_{N=1}^{6} \sum_{T}^{200yr} (WS_{NT} - \overline{WS_{OT}} - \overline{WS_{NO}} + \overline{WS_{OO}})^2$$

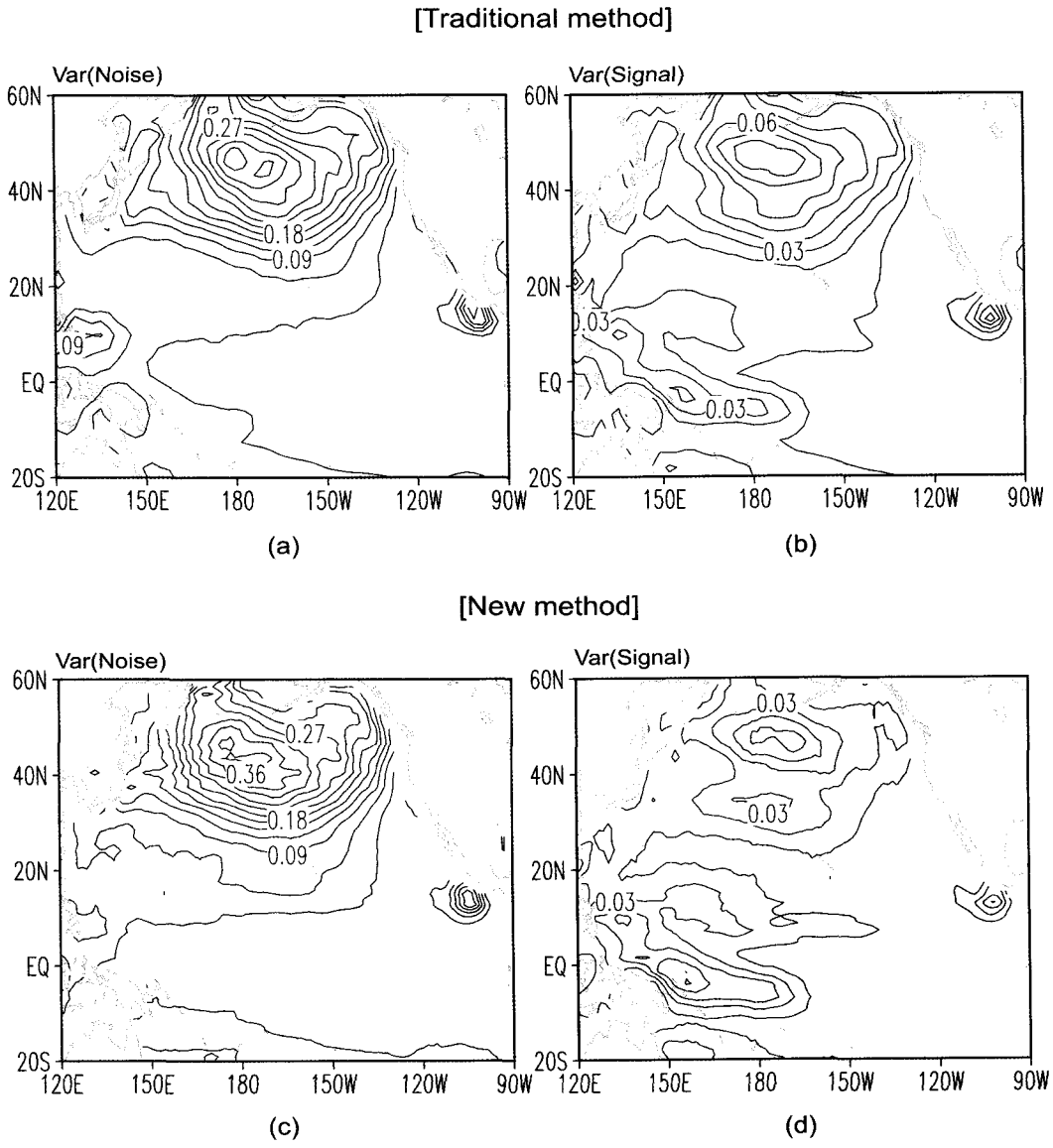

Fig. A1. The noise (a) and signal (b) variability of zonal wind stress based on the traditional method. (c) and (d) as in (a),(b) except for the methodology introduced in section 4. Contour interval is 0.03[dyn/cm^2]^2.

(here, $\overline{WS_{OT}} = \sum_{N=1}^{6} WS_{NT}$, $\overline{WS_{NO}} = \sum_{T}^{200yr} WS_{NT}$)

Figure A1 shows the spatial pattern of the signal and the noise variability for the zonal wind stress calculated from the traditional and our new method, respectively. The pattern of both the signal and the noise are very similar, but the magnitudes are more conservative using our approach. In other words, the signal (noise) is smaller (larger) in our calculation. If we assume that the IE model has only signal (*i.e.* no noise), the magnitude of signal is similar as shown in Fig. A1b. We assert that our approach, which is more conservative, probably gives a more reasonable estimate of the signal and the noise.